



## Hydrodesulfurization enhancement of heavy and light S-hydrocarbons on NiMo/HMS catalysts modified with Al and P



T.A. Zepeda<sup>a,\*</sup>, A. Infantes-Molina<sup>b</sup>, J.N. Díaz de León<sup>a</sup>, S. Fuentes<sup>a</sup>, G. Alonso-Núñez<sup>a</sup>, G. Torres-Otañez<sup>a</sup>, B. Pawelec<sup>b</sup>

<sup>a</sup> Centro de Nanociencias y Nanotecnología, UNAM, Km. 107 Carretera Tijuana-Ensenada, CP, 22800 Ensenada, BC, Mexico

<sup>b</sup> Instituto de Catálisis y Petroleoquímica, CSIC, c/Marie Curie 2, Cantoblanco, 28049 Madrid, Spain

### ARTICLE INFO

#### Article history:

Received 6 March 2014

Received in revised form 29 June 2014

Accepted 30 June 2014

Available online 6 July 2014

#### Keywords:

Hydrodesulfurization

Thiophene

4,6-Dimethylbenzothiophene

Catalysts

Mesoporous materials

Heavy and light S-hydrocarbons

### ABSTRACT

Deep hydrodesulfurization (HDS) of oil fractions is a key process in petroleum refineries due to the increasing demand for S-free diesel and gasoline fractions. In this work, a series of NiMo catalysts supported on Al- and P-modified HMS mesoporous substrate were tested in the HDS of thiophene and 4,6-dimethylbenzothiophene (4,6-DMDBT) to evaluate the effect of Al and P additives on the catalyst response in HDS reactions (thiophene at 1 bar and 4,6-DMDBT at 5.5 MPa). The catalysts were characterized by a variety of techniques (XRD, N<sub>2</sub> adsorption-desorption, TPR, TPS, FT-IR of adsorbed pyridine, UV-vis and H<sub>2</sub> chemisorption). NiMo/Al-HMS-P catalyst containing 1.0 wt.% of P exhibited the best performance in both HDS reactions as a consequence of the proper balance between the active phase dispersion and the largest hydrogenation ability among the studied catalysts. The 4,6-DMDBT HDS reaction proceeded toward direct desulfurization (DDS) and hydrogenation (HYD) reaction routes. Concerning the HDS of thiophene, the increase of the catalyst acidity led to the formation of butadiene and diminished the hydrogenation of olefins (formation of butane). At the reaction temperature of 320 °C, the NiMo/Al-HMS-P1.0 catalyst exhibited the highest activity and the lowest butane formation among the catalysts studied. The isomerization of olefins in the thiophene HDS reaction did not occur, in line with the observed absence of isomerization in the 4,6-DMDBT HDS reaction.

© 2014 Elsevier B.V. All rights reserved.

## 1. Introduction

During the past years the challenge for producing enough hydrocarbon fuels to fulfill the worldwide increasing transportation needs are accentuated by the environmental regulations regarding the sulfur specifications for diesel and gasoline, which have become stricter, and will continue to do so [1–3]. In order to fulfill such requirements, one of the strategies is hydrodesulfurization (HDS) of petroleum feedstock's [4]. This cannot be achieved with the classical Ni(Co)Mo(W)/Al<sub>2</sub>O<sub>3</sub> hydrotreating catalysts due to their thermodynamic limitations for simultaneous deep hydrodesulfurization (HDS) and hydrodearomatization (HDA) at high temperature operation [5]. Thus, it is urgent to develop more efficient catalysts with significantly higher HDS activities than the classical ones [6].

To achieve deep desulfurization of diesel and gasoline, the refractory alkyl-substituted dibenzothiophenes and thiophenic compounds, respectively, should be removed. In particular the

former compounds are very difficult to desulfurize because of the steric hindrance of their alkyl groups, especially when both are in the 4- and 6-positions, for the adequate interaction of the S-atom with the catalytic active site [6]. Since the transformation of those compounds via direct desulfurization reaction route is limited, alternative strategies for elimination of planar configuration of alkyl-substituted DBT involve hydrogenation of their aromatic rings, dealkylation, isomerization and/or C–C bond scission reactions [7]. Contrary to diesel fractions, deep HDS of FCC gasoline is usually accomplished by the use of Ni(Co)Mo(W)/Al<sub>2</sub>O<sub>3</sub> sulfide catalysts. Unfortunately, as the degree of desulfurization increases, the research octane number (RON) of gasoline products decreases due to the hydrogenation of olefins as well as of aromatics present in the feed [8]. Thus, on one hand, sulfur removal from gasoline range (C<sub>4</sub>–C<sub>10</sub>) streams without hydrogenation of olefins remains a significant challenge [8,9]. On the other hand, to enhance the octane number of the gasoline pool, the olefin chain-branching (isomerization) is needed.

It is known that olefins isomerization during HDS of thiophene (through classical or non-classical carbenium chemistry) requires support's acid sites [10]. Thus, to improve the catalyst acid function,

\* Corresponding author. Tel.: +52 6461750650; fax: +52 6461750640.

E-mail addresses: [trino@cny.unam.mx](mailto:trino@cny.unam.mx), [tzepeda@hotmail.com](mailto:tzepeda@hotmail.com) (T.A. Zepeda).

research activities are directed toward the use of strongly acidic supports, such as medium pore ZSM-5 [8] or large pore USY zeolites [9], which demonstrated to be effective for acid-catalyzed reactions such as isomerisation, cracking, hydrotreating and/or alkylation.

Concerning the novel supports, the potential application of highly ordered mesoporous materials, such as MCM-41, SBA-15, HMS or SBA-16, etc., for supporting hydrotreating catalysts has been recently intensively studied [11–13]. This is because their interesting textural properties, such as well-defined uniform mesopores and high surface area, which are particularly attractive for reactions involving large organic molecules [11,12]. Unfortunately, those purely siliceous materials have no Brønsted acidity and limited capacity for ion-change [13]. Thus, considerable efforts have been applied to create acid sites by the substitution of Si<sup>4+</sup> atoms by Al<sup>3+</sup> ions in the pore walls of HMS [14–21], SBA-16 [20,21], MCM-41 [22–28], and SBA-15 [29–35] materials. Among those materials, the hexagonal mesoporous silica (HMS) is of particular interest because it was found that HMS doped with Al, Ti, Zr, etc., exhibited a larger HDS activity than MCM-41 ones in the HDS of DBT [28]. Indeed, the NiMo and CoMo sulfide catalysts supported on Al-HMS demonstrated to be more active in the HDS reaction than their Al-free counterparts [15]. The activity enhancement was explained in terms of the structure and specific electronic properties of the supported active species [15].

Similarly to the support modification with Al<sup>3+</sup>, the increase of the support acidity could be achieved also by support grafting with phosphate [36–41]. Indeed, in the past, this method was the most frequently employed to improve HDS activity of Co(Ni)-Mo(W)/Al<sub>2</sub>O<sub>3</sub> sulfide catalysts [36–41]. However, compared to alumina [36], the effect of P incorporation into the mesoporous siliceous substrate was much less studied and the final conclusions are contradictory [42–49]. In addition, there are also some works reporting no effect, or even negative effect, of phosphorus in the HDS reaction [43,44]. This is probably because the final effect of P-doping is the result of various cumulative effects such as its loading, catalyst preparation method, precursor of active phases and reaction conditions employed. Moreover, the increase of support acidity strongly depends on P loading being the largest acidity achieved for P loadings close to 1.0 wt.% [36–42].

As compared with the support modification with one element or group, the effect of support modification with two additives is scarcely reported [45,46,48]. In this sense, our previous study demonstrated that the post-synthesis modification of Ti-HMS support with phosphorous led to enhancement of dealkylation and isomerization routes of 4,6-DMDBT transformation over CoMo/Ti-HMS-P sulfide catalysts [45]. This prompted us to study the effect of Al-HMS support modification with P on the HDS activity of sulfided NiMo catalysts in deep HDS reactions of model compounds (thiophene and 4,6-DMDBT). To examine the effect of phosphorus concentration on the dispersion of nickel and molybdenum species, and the type of structures formed in the oxide and sulfide form of the P-containing catalysts, the supports and catalysts were characterized by different techniques (XRD, N<sub>2</sub> adsorption–desorption isotherms, DRS UV-vis, TPS, H<sub>2</sub>-TPR, H<sub>2</sub>-chemisorption capability, FTIR spectroscopy of adsorbed pyridine) and tested in the reactions of HDS thiophene and 4,6-DMDBT reactions performed at atmospheric and high hydrogen pressures.

## 2. Experimental

### 2.1. Synthesis of the supports

The Al-HMS support (Si/Al molar ratio of 40) was prepared following the procedure described by Gontier and Tuel [50] using dodecylamine (C<sub>12</sub>H<sub>25</sub>NH<sub>2</sub>, Aldrich 98%) as surfactant and aluminum isopropoxide (98%, Aldrich) as aluminium precursor. The

**Table 1**  
Labeling and nominal composition of the synthesized samples.

Catalysts	Catalyst labeling	Mo (wt.%)	Ni (wt.%)	P (wt.%)
NiMo/Al-HMS 0.0	NiMo-0.0	9.0	3.0	0.0
NiMo/Al-HMS 0.5	NiMo-0.5	9.0	3.0	0.5
NiMo/Al-HMS 1.0	NiMo-1.0	9.0	3.0	1.0
NiMo/Al-HMS 1.5	NiMo-1.5	9.0	3.0	1.5
NiMo/Al-HMS 2.0	NiMo-2.0	9.0	3.0	2.0

Al-HMS solid was air-dried at room temperature for 24 h and subsequently at 110 °C for 2 h. Finally the samples were calcined in air at 500 °C for 4.5 h (heating rate 2.5 °C min<sup>−1</sup>).

Phosphorus was incorporated into Al-HMS by impregnation with an aqueous solutions of H<sub>3</sub>PO<sub>4</sub> using the pore filling method. Thus, an aqueous solution of phosphoric acid (H<sub>3</sub>PO<sub>4</sub>, Fluka 85 wt.% in water) with the corresponding concentration of phosphoric acid was added to the support. These impregnates were dried at room temperature for 16 h, and subsequently at 110 °C for 2 h. Then they were calcined at 500 °C for 4.5 h (heating rate 2.5 °C min<sup>−1</sup>).

### 2.2. Catalyst preparation

The catalysts were prepared by simultaneous impregnation using the pore filling method. An aqueous solution of ammonium heptamolybdate ((NH<sub>4</sub>)<sub>6</sub>Mo<sub>7</sub>O<sub>24</sub>, Aldrich 99%) and nickel nitrate (Ni(NO<sub>3</sub>)<sub>2</sub>, Aldrich 98%), with an appropriate concentration of Ni and Mo, was added to the support. The impregnates were dried at room temperature for 18 h, then at 110 °C for 2 h and finally calcined at 500 °C for 4.5 h (heating rate 2.5 °C min<sup>−1</sup>). Nominal composition and catalysts labeling are given in Table 1.

### 2.3. Characterization methods

#### 2.3.1. X-ray diffraction (XRD)

The X-ray patterns of the calcined and sulfided catalysts were recorded on a Rigaku 2100 diffractometer, using monochromatic CuK<sub>α</sub> radiation ( $\lambda = 0.1541$  nm). The diffractograms were recorded in the 2θ range of 0.15–80° at a step of 0.02°.

#### 2.3.2. N<sub>2</sub> adsorption–desorption isotherms

The textural properties of the supports and oxidic catalysts were determined by N<sub>2</sub> adsorption–desorption isotherms recorded at −196 °C with an ASAP 2000 Micromeritics equipment. The catalysts were sulfided ex-situ in a U-shape glass reactor under the same conditions described in the catalytic activity measurement section. After sulfidation, the sample was cooled to room temperature under N<sub>2</sub> flow and transferred into the Micromeritics apparatus in an Ar atmosphere without exposing the sample to air. Prior to the experiments, the supports and sulfided catalysts were degassed at 270 °C for 5 h. The volume of adsorbed N<sub>2</sub> was normalized to standard temperature and pressure. Specific surface area (S<sub>BET</sub>) was calculated by applying the BET equation to the range of relative pressures 0.05 < P/P<sub>0</sub> < 0.30. The average pore diameter was calculated following the Barret–Joyner–Halenda method (BJH) and using the adsorption branch of the N<sub>2</sub> isotherm. The cumulative pore volume was obtained from the isotherms at P/P<sub>0</sub> = 0.99. The normalized BET area was calculated using the equation:

$$NS_{BET} = \frac{S_{BET} \text{ catalyst}}{(1 - y) \times S_{BET} \text{ support}} \quad (1)$$

where NS<sub>BET</sub> is the normalized S<sub>BET</sub> and y is the weight fraction of the guest phases.

#### 2.3.3. UV-vis diffuse reflectance spectroscopy

The UV-vis diffuse reflectance spectra (DRS UV-vis) of the bare supports and oxide catalyst precursors were recorded using a Cary

$5_E$  spectrophotometer with a specially designed Praying Mantis diffuse reflection attachment (Harrick) for *in situ* measurements. All spectra were recorded after heating the samples at  $250^\circ\text{C}$  in He flow for 1 h. The spectrum of the corresponding support was subtracted from the spectrum of the catalyst. Decomposition of each spectrum was performed by non-linear fitting of multiple Gaussian peak functions sharing a common baseline.

#### 2.3.4. Temperature-programmed reduction ( $\text{H}_2$ -TPR)

TPR experiments of the oxide catalyst precursors were conducted in a Micromeritics 2900 equipment. Prior to reduction, the catalysts (ca. 50 mg) were heated at a rate of  $20^\circ\text{C min}^{-1}$  up to  $400^\circ\text{C}$ , and kept for 2 h under a flow of He to remove water and other contaminants. The catalysts were cooled to room temperature in the same He flow; then reduced in flowing 10%  $\text{H}_2/\text{Ar}$  gas mixture ( $50 \text{ mL min}^{-1}$ ) from r.t. until  $1000^\circ\text{C}$  at a heating rate of  $15^\circ\text{C min}^{-1}$ .

#### 2.3.5. Temperature programmed sulfidation (TPS)

The TPS experiments of the oxide precursors were carried out on Micromeritics ChemiSorb 2720 apparatus, equipped with TCD and UV detectors. Prior to sulfidation, the catalyst (ca. 50 mg) was heated from r.t. until  $300^\circ\text{C}$  at a heating rate of  $20^\circ\text{C min}^{-1}$  and kept at that temperature for 2 h under a flow of He to remove water and other contaminants. Subsequently, the catalysts were cooled to room temperature in the same He flow, and sulfided with heating at a linear temperature ramp ( $15^\circ\text{C min}^{-1}$ ) in flowing 5%  $\text{H}_2\text{S}/\text{H}_2$  gas mixture ( $50 \text{ mL min}^{-1}$ ) from r.t.  $600^\circ\text{C}$ .

#### 2.3.6. $\text{H}_2$ -Chemisorption measurements

The dispersion of the active phase was determined from the amount of chemisorbed  $\text{H}_2$  measured with a pulse method using a Micrometrics ChemiSorb 2720 apparatus. Prior to chemisorption measurements the oxide samples (ca. 50 mg) were reduced *in situ* in an  $\text{H}_2/\text{Ar}$  stream at  $400^\circ\text{C}$  for 2 h, and then cooled in an Ar flow in order to remove physisorbed hydrogen. Pulses ( $0.113 \text{ mL}$ ) of 10%  $\text{H}_2/\text{Ar}$  were injected into a stream of Ar carrier gas ( $50 \text{ mL min}^{-1}$ ) and contacted with the catalyst at room temperature. Metal dispersion was calculated assuming that one Ni and Mo atom chemisorbs one hydrogen atom.

#### 2.3.7. FTIR spectra of adsorbed pyridine

The FT-IR measurements were performed in a Tensor 27 Bruker spectrophotometer. Self-supporting wafers of the oxide catalyst precursor with a thickness of  $12 \text{ mg cm}^{-2}$  were prepared by pressing ( $7 \times 10^3 \text{ kg cm}^{-2}$ ) the powdered sample during 10 min. The wafer was introduced into a special IR cell having greaseless stopcocks and KBr windows. Then the sample was sulfided *in situ* under the same conditions described in the catalytic activity measurement section. The sulfided samples were outgassed at  $450^\circ\text{C}$  for 2 h and cooled down to  $120^\circ\text{C}$  prior to contact with ca. 2 mbar of pyridine. Then, IR spectrum was recorded after evacuation of physically adsorbed pyridine ( $10^{-5} \text{ mbar}$ ) at  $120^\circ\text{C}$  for 0.5 h.

#### 2.3.8. High-resolution transmission electron microscopy (HRTEM)

HRTEM micrographs were collected on a JEOL-2010F instrument. The samples were suspended in heptane as solvent in order to be deposited on lacey carbon (440 mesh) Cu grid holders.

#### 2.4. Catalytic activity measurements

##### 2.4.1. Gas-phase thiophene hydrodesulfurization

The HDS of thiophene was carried out in a vapor phase using a fixed bed micro flow reactor (15 mm ID) housed in a furnace. A quartz reactor was loaded with 100 mg of catalyst (particle size between the 80 and 120 mesh) diluted with 1 g of SiC. Prior to the

catalyst activation by sulfidation, the catalyst was dried under a  $\text{N}_2$  flow of  $100 \text{ mL min}^{-1}$  at  $150^\circ\text{C}$  for 0.5 h. Then, the sample was sulfided with heating up to  $400^\circ\text{C}$ , at a heating rate of  $4^\circ\text{C min}^{-1}$ , in a  $\text{H}_2/\text{H}_2\text{S}$  gas mixture (15% v/v of  $\text{H}_2\text{S}$ ) and kept at this temperature for 2 h. After sulfidation, the catalyst was purged with  $\text{N}_2$  at  $150^\circ\text{C}$  for 0.5 h to eliminate  $\text{H}_2\text{S}$ , which could be adsorbed on the catalyst surface. The reaction was carried out at atmospheric pressure and at different temperatures: 300, 320 and  $340^\circ\text{C}$ . Before the experimental run, the catalytic bed was heated to the desired reaction temperature. Once the test was performed at a given temperature, then the temperature was increased to the next temperature while maintaining the catalyst in a flow of inert gas. Meanwhile, the saturation of hydrogen with thiophene was obtained by bubbling hydrogen ( $50 \text{ mL min}^{-1}$ ) through a saturator containing thiophene liquid at  $0^\circ\text{C}$ . For each catalyst studied, steady state conditions were reached after 1 h of time on-stream reaction. Reaction products were analyzed (by) with an online gas chromatograph (HP-7820, FID) equipped with a CP-Sil 5 CB column. A conventional industrial NiMo/Al<sub>2</sub>O<sub>3</sub> catalyst was tested under the same experimental conditions. This industrial reference sample has a chemical composition of 12, 4 and 2.4 wt.% of Mo, Ni and P, respectively. The textural properties for the reference sample are the follows:  $215 \text{ m}^2 \text{ g}^{-1}$ ,  $0.45 \text{ cm}^3 \text{ g}^{-1}$  and  $7.6 \text{ nm}$  of  $S_{\text{BET}}$ , cumulative pore volume and average pore diameter, respectively.

##### 2.4.2. 4,6-Dimethylbibenzothiophene hydrodesulfurization

The catalytic activity was evaluated in the reaction of HDS of 4,6-DMDBT (300 ppm of S) carried out in a batch Parr reactor (300 mL capacity) charged with 0.2 g of catalyst (particle size between  $-80/+100$  mesh) and 0.3 g of 4,6-DMDBT dissolved in 100 mL of *n*-dodecane. The reaction was carried out at  $320^\circ\text{C}$  under a total  $\text{H}_2$  pressure of  $5.5 \text{ MPa}$  for 6 h. Before the activity test, the catalyst was sulfided in a U-shape glass flow reactor. First the sample was flushed in a nitrogen flow gradually increasing the temperature from room temperature up to  $150^\circ\text{C}$  for 0.5 h. Then, the sample was sulfided with a 15% v/v of  $\text{H}_2\text{S}$  gas mixture ( $60 \text{ mL min}^{-1}$ ) from  $150^\circ\text{C}$  up to  $400^\circ\text{C}$  (heating rate of  $4^\circ\text{C min}^{-1}$ ), and kept at this temperature for 2 h. After sulfidation, the catalyst was purged with  $\text{N}_2$  at  $150^\circ\text{C}$  for 0.5 h to eliminate  $\text{H}_2\text{S}$ , which could be adsorbed on the catalyst surface. After cooling down to room temperature, the sulfided sample was transferred to the batch reactor in an argon atmosphere with the aim to avoid contact with air. The reaction products were analyzed by GC on a Perkin-Elmer XL equipment using 30 m capillary column coated with a non-polar methyl silicone phase (DB-1, J & W). For comparison purpose, the activity of a conventional industrial NiMo/Al<sub>2</sub>O<sub>3</sub> catalyst was tested under the same experimental conditions. This industrial reference sample has a chemical composition of 12, 4 and 2.4 wt.% of Mo, Ni and P, respectively. The textural properties for the reference sample are the follows:  $215 \text{ m}^2 \text{ g}^{-1}$ ,  $0.45 \text{ cm}^3 \text{ g}^{-1}$  and  $7.6 \text{ nm}$  of  $S_{\text{BET}}$ , cumulative pore volume and average pore diameter, respectively.

### 3. Results and discussion

#### 3.1. Textural properties

The values of specific BET surface area ( $S_{\text{BET}}$ ), total pore volume and pore diameter of bare supports and oxide catalyst precursors are listed in Table 2. Fig. 1 shows the influence of P loading on the specific BET surface area and total pore volume of the bare supports and oxide catalyst precursors. For the bare substrates, Al-HMS P-loaded samples suffer a decrease in the specific BET area ( $S_{\text{BET}}$ ) and pore volume suggesting a partial blockage of pores by P species. As expected, the NiMo-2.0 sample shows the largest decrease of  $S_{\text{BET}}$  and total pore volume among the studied catalysts. A further

**Table 2**

Textural properties of pure supports and oxide precursors as determined by  $N_2$  adsorption desorption isotherms<sup>a</sup> at  $-196^\circ\text{C}$  and low-angle XRD diffraction patterns<sup>b</sup>.

Sample	$S_{\text{BET}}$ ( $\text{m}^2 \text{g}^{-1}$ )	$d_p$ (nm)	$V_p$ ( $\text{cm}^3 \text{g}^{-1}$ )	$NS_{\text{BET}}$	$d_{100}$ (nm)	$a_0$ (nm)	wt (nm)
Supports							
Al-HMS-P 0.0	1013	3.1	1.17	—	7.18	8.29	5.19
Al-HMS-P 0.5	1021	3.1	1.01	1.00	6.54	7.55	4.45
Al-HMS-P 1.0	994	3.0	0.98	0.99	6.40	7.39	4.39
Al-HMS-P 1.5	972	3.0	0.93	0.97	6.74	7.78	4.78
Al-HMS-P 2.0	901	2.9	0.88	0.90	6.13	7.08	4.18
Oxide precursors							
NiMo-0.0	796	3.1	1.01	0.89	6.35	7.33	4.23
NiMo-0.5	723	3.0	0.94	0.80	6.54	7.55	4.55
NiMo-1.0	691	3.0	0.89	0.79	6.09	7.03	4.03
NiMo-1.5	668	3.1	0.83	0.78	5.77	6.66	3.56
NiMo-2.0	604	2.7	0.75	0.76	5.42	6.25	3.55

<sup>a</sup>  $S_{\text{BET}}$ : specific surface area;  $d_p$ : pore diameter;  $V_p$ : total pore volume;  $NS_{\text{BET}}$ : normalized BET surface area calculated using Eq. (1).

<sup>b</sup>  $d_{100}$ ,  $d$ -Spacing as calculated from the X-ray patterns;  $a_0$ , unit cell parameter estimated from the position of the (100) diffraction line and calculated employing equation  $a_0 = d_{100} \times 2/\sqrt{3}$ ; wt, wall thickness was obtained by subtracting pore diameter ( $d_p$ ) from the unit cell parameter.

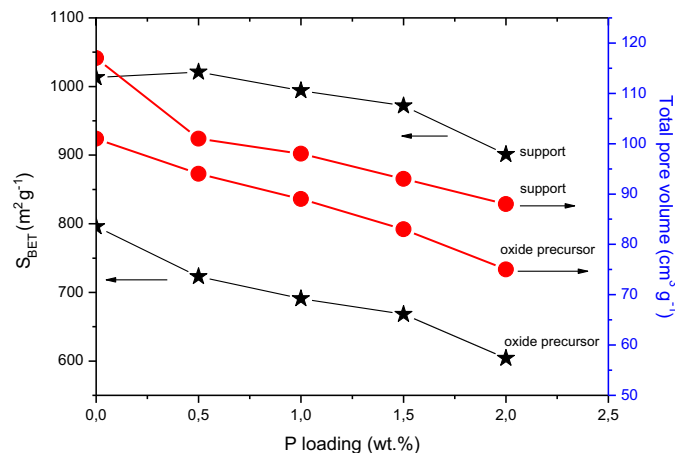


Fig. 1. Influence of P loading on the specific BET surface area and total pore volume of the pure Al-HMS-P supports and oxide NiMo/Al-HMS-P catalyst precursors.

decrease in the  $S_{\text{BET}}$  is observed after Ni and Mo incorporation due to a progressive blockage of the support's pores by the metal oxide particles formed during calcination.

To get an idea about the location of the guest phases in the support structure, the normalized  $NS_{\text{BET}}$  of the supports and the corresponding catalysts have been calculated (Eq. (1)), and the corresponding values are included in Table 2. The values corresponding to pure supports ranged from 0.9 to 1.0 pointing to a homogeneous location of P species on both the support surface and within the inner porous structure. After Ni and Mo addition, a further decrease is observed. The catalyst without P, NiMo-0.0 presents the highest value 0.89, indicating the main location of the active phase in the outer surface. By increasing the P loading, the catalysts containing 0.5, 1.0, 1.5 and 2.0 possess lower values although the differences between them are very low. These data suggest that P favors the incorporation of the active phase into the mesoporous structure. The lowest  $NS_{\text{BET}}$  value recorded for the catalyst containing the highest P-loading suggests that Ni-Mo species are located not only inside the pores but also at the entrance of the mesopores.

### 3.2. XRD

As the HMS substrate shows wormhole hexagonal ordered mesoporous structure [50] low angle XRD analyses were performed to reveal whether or not this structure is preserved after support treatment with phosphoric acid and its further impregnation with metal oxide precursors. The low-angle XRD patterns

of pure supports and oxide precursors are shown in Fig. 2(A) and (B), respectively. In all cases, the diffractograms present a broad reflection peak at  $2\theta=1.0\text{--}2.0^\circ$  that can be indexed to the  $d_{100}$  reflection of a 2D hexagonal structure that is characteristic of the HMS systems and therefore indicative of the maintenance of the mesoporous structure after the impregnation and calcination processes. The comparison of patterns of oxide catalyst precursors reveals that the diffraction peak becomes less intense and broader and shifts to higher angles, from  $1.37^\circ$  in NiMo-0.0 to  $1.57^\circ$  in NiMo-2.0. These data indicate a partial collapse of the HMS mesoporous structure upon P, Ni and Mo incorporation. In this regard, by calculating the  $d$ -spacing values of the samples (Table 2), it decreases with the P content and in a greater extent after the incorporation of Ni and Mo species. Thus, the  $d_{100}$  values change from 7.18 nm for the support without P (Al-HMS-P0.0) to 6.13 nm for the support containing the highest P loading (Al-HMS-P2.0). A similar trend is observed for the oxide catalyst precursors. The  $a_0$  and wall thickness present the same tendency. For pure supports, a decrease of the cell parameter and wall thickness with an increase of P loading suggest some collapse of the support structure upon support's treatment with phosphoric acid (Table 2). Similarly, the incorporation of the metal oxides followed by calcination led to a further decrease of both unit cell parameter and wall thickness with respect to the original support values indicating some collapse of pore structure.

### 3.3. DRS UV-vis spectra

Information about the distribution of Mo oxide species on the supports, and therefore their dispersion, was also evaluated by UV-vis DRS spectra (Fig. 3). The spectrum of each support was subtracted from the spectrum of the corresponding NiMo catalyst. The bands in the 260–280 nm range are due to  $\text{O}^{2-}\text{-Mo}^{6+}$  ligand-to-metal charge transfer transition (LMCT) in tetrahedral coordination of isolated molybdate species ( $\text{Mo}_{\text{Th}}$ ); the bands in the 300–370 nm range are due to polymolybdate octahedral ( $\text{Oh}$ ) Mo species ( $\text{Mo}_{\text{Oh}}$ ); moreover, both types of  $\text{Mo}^{6+}$  species show a second absorption band at about  $230\text{ cm}^{-1}$  [51]. As seen in Fig. 2, all the catalysts show a similar profile, with a strong absorption band at ca.  $230\text{--}240\text{ cm}^{-1}$  indicative of the coexistence of a mixture of  $\text{Mo}^{6+}$  species in octahedral and tetrahedral coordination. Deconvolution of all these spectra gives rise to two absorption bands located at ca.  $244$  and  $302\text{ cm}^{-1}$  whose relative intensity depends on the P content. In all cases, mixtures of  $\text{Mo}_{\text{Th}}$  and  $\text{Mo}_{\text{Oh}}$  are present, although the proportion of tetrahedral Mo species is much more important than octahedral ones. In the NiMo-0.0 sample the contribution of  $\text{Mo}_{\text{Th}}$  species is the most important while a tiny absorption band due to  $\text{Mo}_{\text{Oh}}$  is observed. Upon P incorporation, the band due to

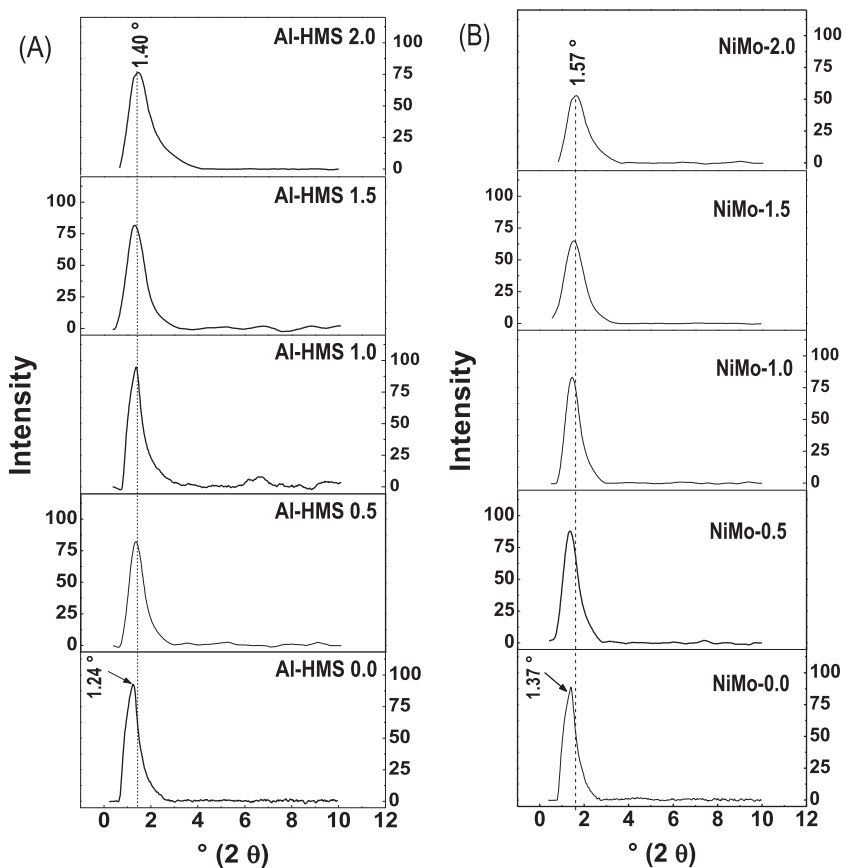


**Fig. 2.** Low-angles X-ray diffraction patterns of the pure supports (A) and oxide catalyst precursors (B).

$\text{Mo}_{\text{Th}}$  species becomes narrower and shifts to lower wavelengths, while the contribution of  $\text{Mo}_{\text{Oh}}$  ones increases in intensity, becoming a distinguishable shoulder of the  $\text{Mo}_{\text{Th}}$  absorption for NiMo-1.0, NiMo-1.5 and NiMo-2.0 samples. As the position of the absorption bands is related to the coordination and agglomeration degree of

Mo species, it can be inferred that  $\text{Mo}_{\text{Th}}$  species are better dispersed over these samples, besides they also present a greater proportion  $\text{Mo}_{\text{Oh}}$  ones. The exception is NiMo-2.0 which in spite of presenting a greater amount of  $\text{Mo}_{\text{Oh}}$  species, the peak positions are similar to that of P-free sample, indicating that the dispersion is worse than for the other P-containing catalysts.

### 3.4. $\text{H}_2$ -TPR experiments

The influence of P on the reducibility of nickel and molybdenum species was studied by  $\text{H}_2$ -TPR. The corresponding profiles are depicted in Fig. 4. The TPR profiles of all NiMo/Al-HMS-P(x) samples show two main reduction peaks. The first one located at 527 °C in all the samples, and a second one at higher temperatures, whose position depends on P content. Thus, for the P-free sample this second peak is located at 745 °C but it shifts to higher temperature upon increasing P-loading. In addition, another band is observed at intermediate temperatures, ca. 600 °C, and seen as a shoulder of the low temperature peak. This band becomes better defined for the P-free sample (NiMo-0.0). The peak located at 527 °C can be ascribed to the reduction,  $\text{Mo}^{6+}$  to  $\text{Mo}^{4+}$ , of polymeric octahedral Mo species,  $\text{Mo}_{\text{Oh}}$ , weakly bounded to the support surface [51,52]. The position of this peak does not change under phosphorous presence but becomes narrower and more intense, except for NiMo-2.0 sample. These data suggest that the interaction of  $\text{Mo}_{\text{Oh}}$  species does not depend on the P presence but their amount increases, as previously observed by UV-vis DRS spectra. The shoulder at 600 °C has been previously ascribed to reduction of  $\text{Ni}^{2+}$  ions in tetrahedral coordination ( $\alpha\text{-NiMoO}_4$  phase) [15] taking into account that the reduction peak of  $\text{Ni}^{2+}$  ions in octahedral coordination overlaps with that of  $\text{Mo}^{6+}$ . This contribution is less important when P is present, suggesting that P inhibits to a some extent the formation

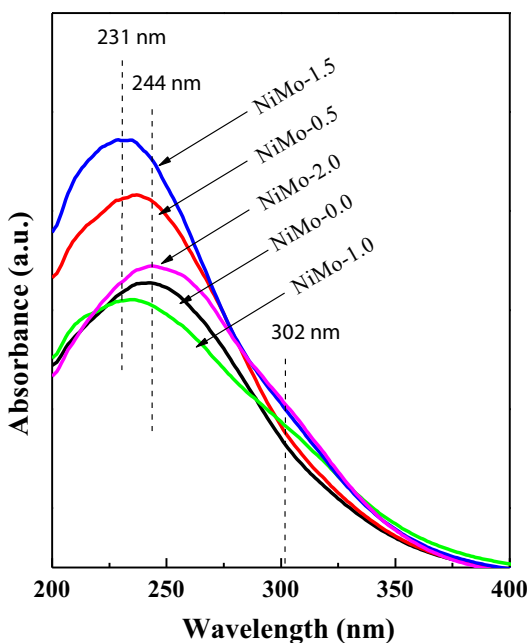


**Fig. 3.** DRS UV-vis spectra of the NiMo/Al-HMS and NiMo/Al-HMS-P(x) oxide catalyst precursors.

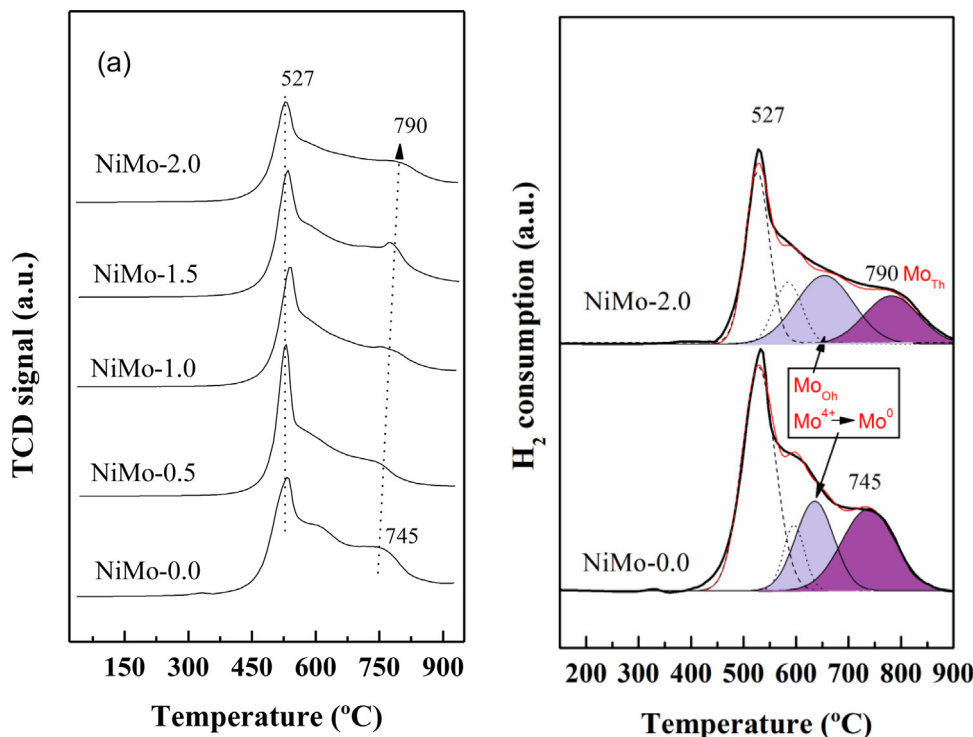


**Fig. 4.** (a) TPR profiles of the NiMo/Al-HMS-P(x) oxide precursors. (b) Gaussian deconvolution of the TPR profiles of NiMo-2.0 and NiMo-0.0 samples.

of Ni<sup>2+</sup> in tetrahedral coordination. Finally, the reduction peak at higher temperature (750 °C) corresponds to the second reduction step of polymeric octahedral molybdenum species (Mo<sup>4+</sup> to Mo<sup>0</sup>) and to the first step of reduction of isolated tetrahedral molybdates (Mo<sub>Th</sub>) strongly interacting with the support [53]. This reduction process is less important and shifts to higher temperatures under the presence of P, from 750 °C for NiMo-0.0 to 790 °C for NiMo-2.0. These data indicate that P favors the formation of a higher amount of Mo<sub>Oh</sub> species, and therefore it reduces the proportion of unreduceable Mo species (Mo<sub>Th</sub>), even though they become reduced at higher temperatures.

### 3.5. TPS experiments

Fig. 5 shows the H<sub>2</sub>S consumption profiles observed during TPS experiments of supports (dashed lines) and oxide precursors (continuous lines). All supports presented more or less the same general behavior. Physically adsorbed H<sub>2</sub>S was released at temperatures above 100 °C. The maximum of this peak was observed at 150 °C for P-free, NiMo-0.5 and NiMo-2.0 catalysts but it shifted to higher temperatures for NiMo-1.0 and NiMo-1.5 ones. All the supports presented a broad H<sub>2</sub>S consumption band at around 400 °C.

The TPS of the oxide precursors also presented a desorption peak similar to that observed for the P-free sample. The total amount of consumed H<sub>2</sub>S increased with P-content catalysts until 1.0% and then it decreased for NiMo-1.5 catalyst after which the amount of consumed H<sub>2</sub>S again increased for NiMo-2.0 sample. All catalysts exhibited at least two peak maxima. For the P-free material the first consumption peak at around 346 °C is attributed to the exchange of sulfur for oxygen in MoO<sub>3</sub> to produce MoO<sub>2</sub>S and water [54]. After this process a decomposition-reduction process of the oxysulfide species formed has been reported to produce MoO<sub>2</sub>. However it cannot be observed directly from the depicted TPS patterns since it should be accompanied by a negative H<sub>2</sub>S consumption peak arising from the hydrogenation of elemental sulfur and the resulting H<sub>2</sub>S production, thus indicating that this band is not well resolved

and overlaps with the sulfidation process. The second H<sub>2</sub>S consumption peak at around 430 °C corresponds to the sulfidation process of MoO<sub>2</sub> to produce the MoS<sub>2</sub> active phase. The TPS patterns of the catalysts containing P showed more or less the same general behavior as the described for P-free catalyst, nevertheless some differences aroused as the P loading varied. In the case of the NiMo-0.5 catalyst three peaks were observed, suggesting the presence of MoO<sub>3</sub> particles that exhibit different interaction strengths with the support. When P was increased to 1.0 wt.% both an increase in the amount of H<sub>2</sub>S consumption and a decrease in the temperature of the first consumption peak were observed. This indicates a larger amount of MoS<sub>2</sub> sulfided species with weaker active phase-support interactions. For the NiMo-1.5 catalyst the observed TPS pattern was very similar to that of the NiMo-1.0 sample but a considerably lower H<sub>2</sub>S consumption was observed in the low temperature peak. Finally, the NiMo-2.0 catalyst showed two main peaks located around 270 °C and 400 °C. Again, this shift to lower temperatures indicates a weaker metal-support interaction than that observed for the P-free catalyst.

### 3.6. Characterization of sulfided catalysts

#### 3.6.1. XRD

XRD measurements were used to study the crystalline phases of sulfided catalysts. The diffraction patterns of sulfide catalysts in Fig. 6 shows the same general features and reveal that the structure of HMS substrate apparently is not modified by P introduction. Moreover, no diffraction peaks corresponding to any phosphate phase are observed. All samples present a broad peak between 18 and 32° (2θ) which is attributed to the amorphous part of the Al-HMS supports. Diffraction peaks located at 14.4, 33.1, 36.0, 39.5, 49.8 and 58.3° (2θ) belong to MoS<sub>2</sub> crystallites (JCPDS card 37-1492). Upon increasing P content until 1 wt.% the diffraction peaks of MoS<sub>2</sub> are less intense than in the P-free sample suggesting a loss of crystallinity and a better dispersion of the MoS<sub>2</sub> crystallites formed. The crystallite sizes were estimated using the Scherrer

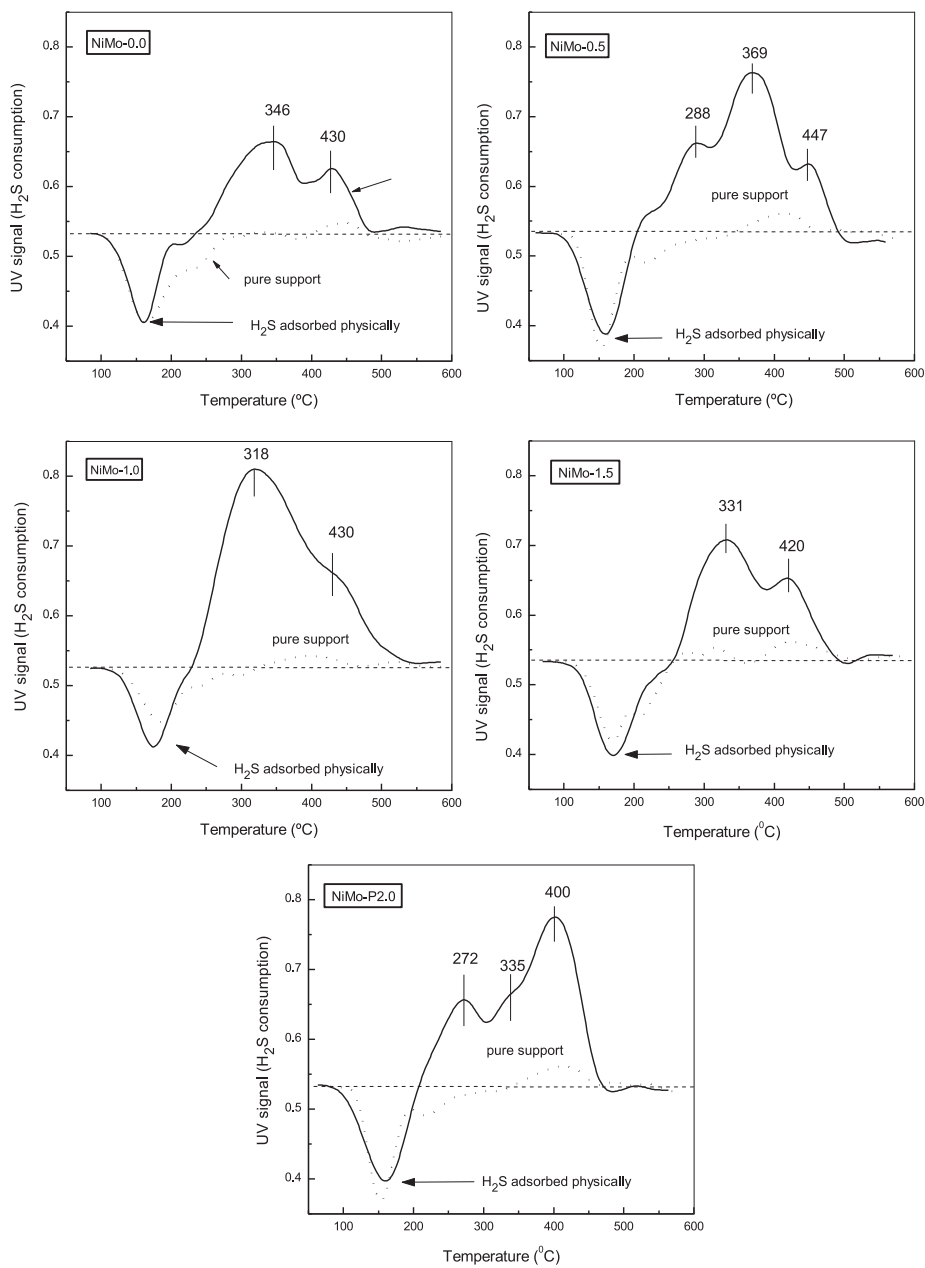


**Fig. 5.** TPS profiles of the oxide catalyst precursors.

equation for the highest intensity diffraction peak located at 14.4° corresponding to the (0 0 2) plane. Crystallite sizes increased in the order: NiMo-1.0 (12.8 nm) < NiMo-2.0 (17.1 nm) < NiMo-0.5 (20.8 nm) < NiMo-0.0 (25.7 nm). No diffraction peaks of other crystalline than MoS<sub>2</sub> phase were recorded.

### 3.6.2. H<sub>2</sub>-chemisorption measurements

The dispersion of the oxide Ni-Mo species exposure was determined by H<sub>2</sub> chemisorption measurements. The obtained values are included in Table 3. As observed from XRD measurements, the presence of phosphorous improves the Ni-Mo dispersion. Thus an increment of P content until 1.0–1.5 wt.% increases the metallic dispersion from 13% to 17%. However, further addition of P (2.0 wt.%) provokes a drastic decrease of metallic dispersion to 8.7%. These results are in agreement with the tendency observed in the textural properties, where no important changes in dispersion are observed until 1.0 wt.% of P, on the contrary dispersion drops severely upon increasing P-loading.

**Table 3**

Chemisorption capacity and metal dispersion of the NiMo-P(x) freshly sulfided catalysts as determined by H<sub>2</sub> chemisorption.

Sample	H <sub>2</sub> uptake <sup>a</sup> (μmol g <sub>cat</sub> <sup>-1</sup> )	Dispersion <sup>a</sup> (%)
NiMo-0.0	73	13.1
NiMo-0.5	96	13.8
NiMo-1.0	112	17.2
NiMo-1.5	105	16.8
NiMo-2.0	66	8.7

<sup>a</sup> Chemisorption capacity as determined by pulse method of H<sub>2</sub> chemisorption in the oxidized catalysts.

### 3.6.3. FT-IR spectra of adsorbed pyridine

FT-IR spectra of adsorbed pyridine on sulfide catalysts were recorded with the objective to reveal acidity differences between P-free and P-containing samples. Fig. 7 shows the infrared spectra of the pyridine adsorbed on P-free and P-containing sulfide catalysts. All catalysts show similar spectra in the range 1400 to 1650 cm<sup>-1</sup>.

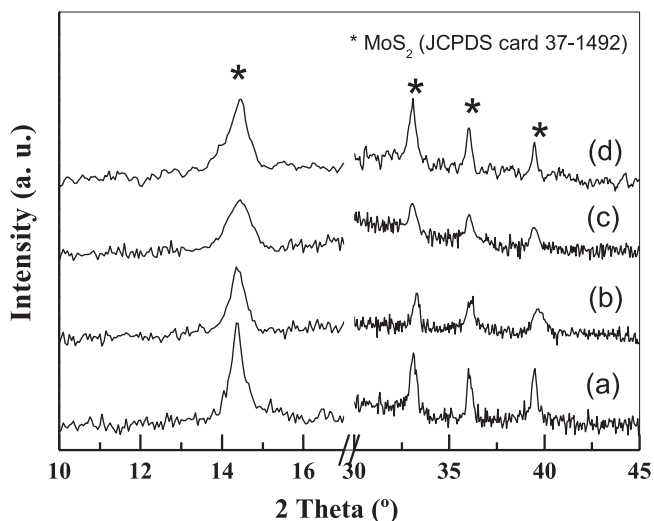


**Fig. 6.** X-ray diffraction patterns of fresh sulfided catalysts: (a) NiMo-0.0; (b) NiMo-0.5; (c) NiMo-1.0, and (d) NiMo-2.0.

Two strong bands assigned to the pyridine chemisorbed on Lewis sites and hydrogen-bonded pyridine is observed at 1445 and 1600 cm<sup>-1</sup>, respectively [55]. A small band located at 1542 cm<sup>-1</sup> is assigned to the vibration mode of pyridinium ion adsorbed on Brønsted sites while a band observed at 1486 cm<sup>-1</sup> is assigned to pyridine associated with both Lewis and Brønsted sites [56]. The P-free sample presents the bands at 1571 and 1445 cm<sup>-1</sup> of weak and strong adsorbed pyridine on Lewis sites, respectively, and a small one at 1542 cm<sup>-1</sup> due to Brønsted acid sites, indicating that the main acid sites on sulfided NiMo-0.0 catalyst are of Lewis nature. Upon P addition, the intensity of these bands increases suggesting that the incorporation of P increases the population of

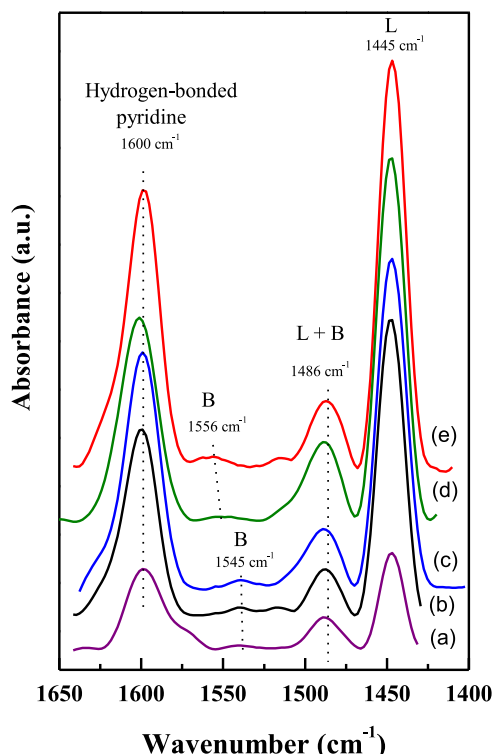


**Fig. 7.** FT-IR spectra of adsorbed pyridine on the NiMo/Al-HMS-P(x) sulfide catalysts: (a) NiMo-0.0; (b) NiMo-0.5; (c) NiMo-1.0; (d) NiMo-1.5; (e) NiMo-2.0. B, Brønsted acid sites; L, Lewis acid sites.

**Table 4**

Effect of support functionalization with  $-\text{PO}_3\text{H}_2$  groups of NiMo-P(x) sulfided catalysts on the amount of Brønsted and Lewis acid sites<sup>a</sup>.

Catalyst	Brønsted ( $\mu\text{mol g}_{\text{cat}}^{-1}$ )	Lewis ( $\mu\text{mol g}_{\text{cat}}^{-1}$ )
NiMo-0.0	0.4	2.8
NiMo-0.5	0.2	11.0
NiMo-1.0	0.2	13.7
NiMo-1.5	0.2	13.4
NiMo-2.0	1.1	15.9

<sup>a</sup> As determined by FTIR spectroscopy of adsorbed pyridine.

Lewis acid sites. Thus, from FT-IR spectra the quantitative analysis of Brønsted and Lewis acidity was done as reported in [57] and the corresponding amount of each acid site-type Lewis (L) and Brønsted (B)) are reported in Table 4. The amount of Brønsted acid sites was much lower than the estimated concentration of Lewis sites, regardless the P content in the catalyst and always lower under the presence of P, with the exception of NiMo-2.0 sample. Instead, a considerable increase in Lewis acidity occurs after the addition of 0.5 wt.% of P to the support. Further addition of P also increases the population of Lewis acid sites, but to a lesser extent. As seen in Table 4, the Brønsted acidity trend is: NiMo-2.0 > NiMo-0.0 > NiMo-0.5 = NiMo-1.0 = NiMo-1.5. Thus, the NiMo-2.0 sample displays the largest amount of both Brønsted and Lewis acid sites among the catalysts studied.

Summarizing the catalyst characterization data, we conclude that support modification with phosphorous has a detrimental effect on the textural properties because it decreases specific surface area and collapses partially the Al-HMS mesoporous structure, as confirmed by N<sub>2</sub> physisorption and low-angle XRD, respectively. Moreover, it was found that the Lewis acidity depends strongly on the amount of phosphorous incorporated over the support. On the contrary, the phosphorus addition on the support did not influence on the Brønsted acid sites. For the NiMo-0.5, NiMo-1.0 and NiMo-1.5 samples, the Brønsted acidity decreases with respect to P-free counterpart. This is suggesting a multiple bonding of phosphoric acid to three different hydroxide groups of the support [38]. However, an important increment in the Brønsted acidity was observed in the NiMo-2.0 sample. This could relate that the hydroxyl groups bonded to tetrahedral Si<sup>4+</sup> ions acts as Brønsted acid sites, considering one point bonding of the phosphoric acid to one hydroxyl group of the carrier, as it was suggested by Fitz and Rase [38]. On the contrary to acidity, the presence of P species on the support surface enhances both the dispersion of metal oxide species and their reducibility, as deduced from XRD and TPR data, respectively. The calculation of the normalized S<sub>BET</sub> (expressed as m<sup>2</sup> g<sup>-1</sup> of support) of the catalyst indicated the homogeneous distribution of metal oxide species within the inner pores of the support and on their surface. Upon sulfidation, all catalysts show the formation of MoS<sub>2</sub> phase being nickel species so small to be detected by XRD (Fig. 6). This technique also shows that a large amount of phosphate (2.0 wt.%) favors the particles growth due to excessive weakening of the metal-support interaction deduced from TPS measurements (Fig. 5).

In this sense, the morphology for the some sulfided samples was studied by statistical calculation of ca. 500 particles from 12 HRTEM micrographs. HRTEM images of sulfided NiMo-0.0 and NiMo-1.0 catalyst are shown in Fig. 8(a) and (b), respectively. One can observe that the stacking in both samples is closed at 4. Nonetheless, an important effect on the dispersion and sulfide slabs size were enhancement with the phosphorus addition. The catalyst prepared on the phosphate support modification has the lower average size of the slabs value of  $2.2 \pm 0.25$  nm, which represents 2.9 nm obtained for the free phosphorus containing sample. The surface density of MoS<sub>2</sub> slabs was also calculated. The surface density of the slabs for the 1 wt.% P-containing sample was of 1 MoS<sub>2</sub>

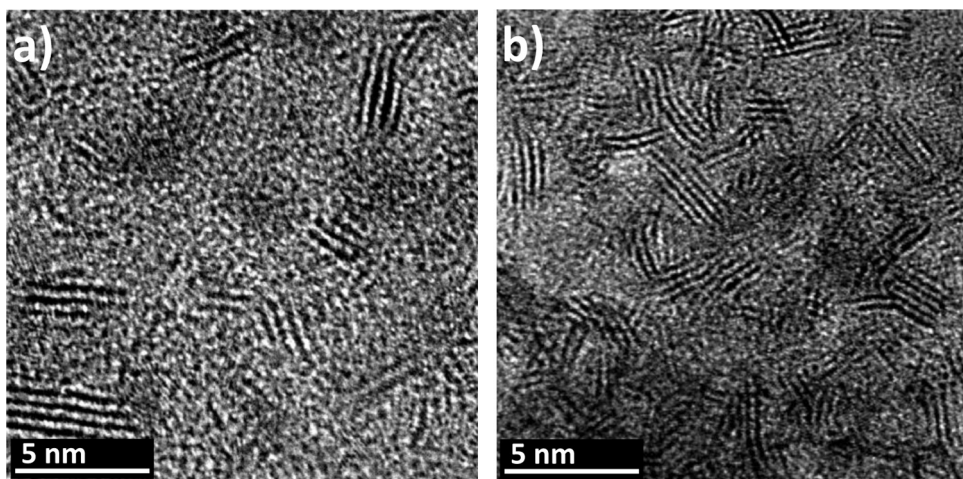


**Fig. 8.** HRTEM images of the sulfide NiMo-0.0 and NiMo-1.0 samples.

slabs (particle)/10 nm<sup>2</sup>, while for the P-free catalyst was of 1 MoS<sub>2</sub> slabs (particle)/25 nm<sup>2</sup>. These displayed values confirm a high dispersion of the active phase in the sample with 1 wt.% of phosphorus. These results are in agreement with the discussed previously.

### 3.7. Catalytic results

In the present study, NiMo/Al-HMS-P(x) catalysts were tested in the HDS of thiophene (TF) and 4,6-dimethylbenzothiophene (4,6-DMDBT); the later sulfur-containing molecule is considered as representative of the refractory sulfur compounds contained in the gas oil fraction. For comparative purposes a reference NiMo catalyst was also tested (NiMo/Al<sub>2</sub>O<sub>3</sub>).

#### 3.7.1. HDS of thiophene

The activity of NiMo-0.0, NiMo-1.0 and NiMo-2.0 sulfide catalysts was evaluated in the HDS of thiophene at 300, 320 and 340 °C at atmospheric pressure. The influence of the reaction temperature and P loading on the thiophene conversion are shown in Fig. 9(a). From this results we the activation energies were estimated for each sample, the  $E_a$  values were 24.7, 30.4, 28.7 and 27.9 kJ mol<sup>-1</sup> for the NiMo-0.0, NiMo-1.0, NiMo-2.0 and NiMo/Al<sub>2</sub>O<sub>3</sub> samples, respectively. The activation energies values follow the trend: NiMo-1.0 > NiMo-2.0 > NiMo/Al<sub>2</sub>O<sub>3</sub> > NiMo-0.0. This trend indicates that activity increases upon P incorporation up to 1.0 wt.% of P and then declines at higher P-loading. It can be noted that the commercial NiMo/Al<sub>2</sub>O<sub>3</sub> catalysts is less active than NiMo-1.0 one.

The influence of the reaction temperature on product selectivity, taken to a thiophene conversion of 20–25%, is shown in Fig. 10. Under the reaction conditions employed, the reaction products identified were *n*-butane, 1-butene and *cis* and *trans*-butene for P-free catalyst (NiMo-0.0) and also 1,3 butadiene for the other catalysts. As expected, the product selectivity strongly depends on the reaction temperature and catalyst composition. The general trend observed is the increase of butane and 1-butene selectivity and a decrease of 2-butenes and 1,3 butadiene with temperature. The proportion of each one depends on catalyst composition. Thus, NiMo-0.0 produces the highest amount of butane and 1-butene. However, 1,3-butadiene is formed upon P-adding to the catalyst, mainly at low temperatures because it becomes hydrogenated at higher temperatures. Besides, a considerable increase of 2-butenes selectivity is also observed upon P addition (mainly over NiMo-1.0).

Phosphorus it also has an important effect on selectivity, considering the olefins/paraffin ratio ((butenes + butadiene)/butane) (Fig. 9(b)), in both P-containing samples the olefins selectivity was

higher than the P-free catalyst, probably related with the higher acidity measure for these samples. This is an important finding because our objective in this work is to diminish olefins hydrogenation. At a reaction temperature of 300 °C, both NiMo-2.0 and NiMo/Al<sub>2</sub>O<sub>3</sub> samples showed very low HYD capability. However, an increase of the reaction temperature led to the undesirable enhancement of olefin hydrogenation for all the catalysts studied. Besides this, it is also noted that the most active NiMo-1.0 catalyst displayed larger olefin/butane ratio than its NiMo-0.0 and NiMo-2.0 counterparts. However, regardless the reaction temperature, its selectivity toward butane formation is larger than that of the

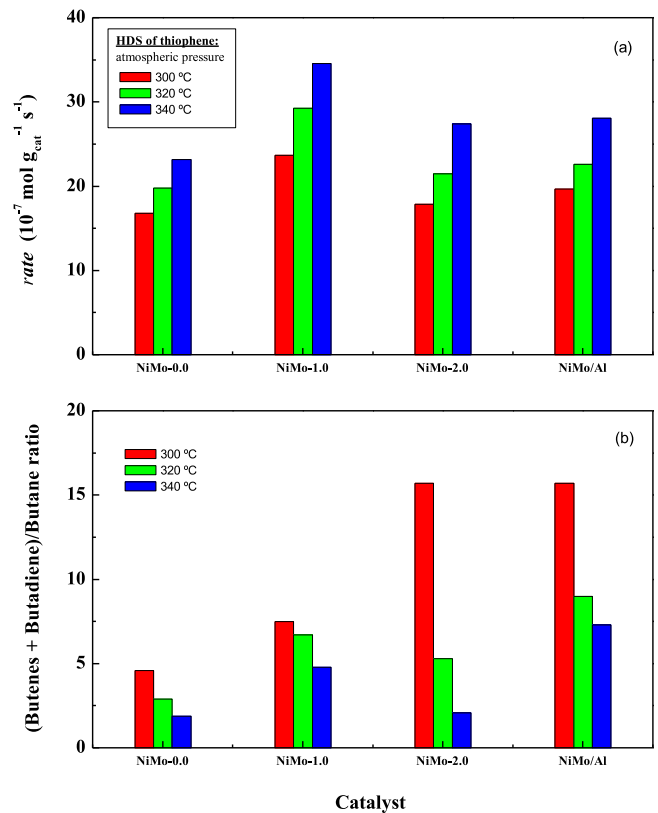


**Fig. 9.** HDS of thiophene over NiMo/Al-HMS and NiMoAl-HMS-P(x) sulfide catalysts (a flow reactor, a steady-state; atmospheric pressure,  $T = 300, 320, 340$  °C and conversions between 20 and 25%). Influence of the reaction temperature and P loading on catalyst activity (a) and the comparison of olefins/butane ratio (b).

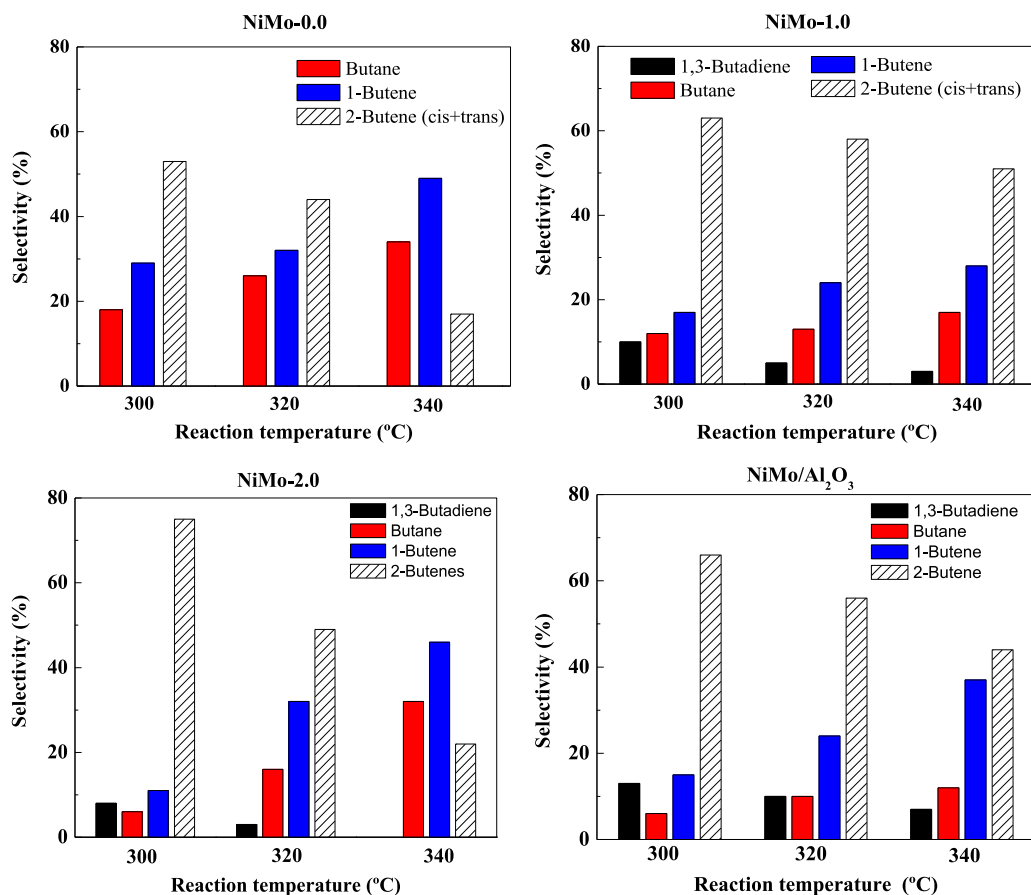
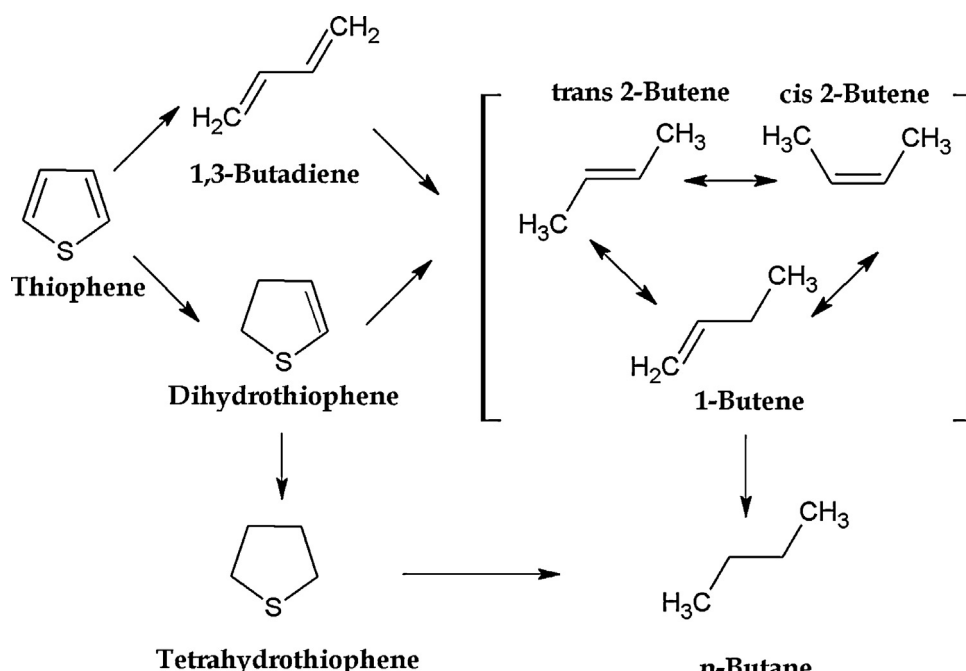


**Fig. 10.** Influence of the reaction temperature on the selectivity of products in the HDS of thiophene over sulfide catalysts (atmospheric pressure;  $T = 300, 320, 340^\circ\text{C}$ ; steady-state, a flow reactor).



**Scheme 1.** Reaction scheme for the hydrodesulfurization of thiophene over NiMo/Al-HMS-P(x) sulfide catalysts.

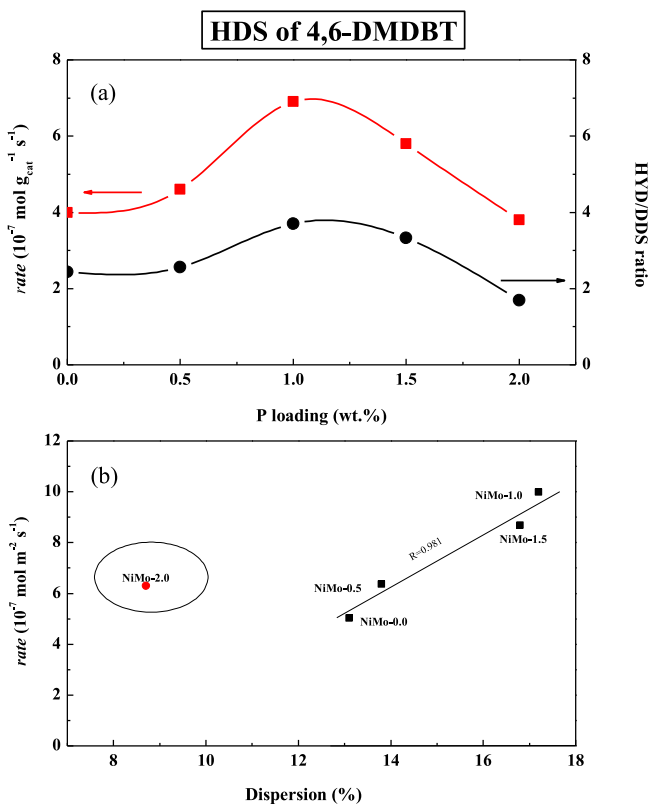


**Fig. 11.** HDS of 4,6-DMDBT DMBT ( $P=5.5 \text{ MPa}$ ;  $T=320^\circ\text{C}$ , reaction time of 6 h; a batch reactor) over NiMo/Al-HMS and NiMo/Al-HMS-P(x) sulfide catalysts. Influence of the P loading on the activity and selectivity (a). Influence of the active phase dispersion (from  $\text{H}_2$  chemisorption) on the HDS activity of catalysts (b).

reference catalyst. It is noteworthy that for all catalysts studied the olefin chain-branched did not occur. **Scheme 1** shows the possible HDS reaction mechanism over P-containing catalysts and the reference one. 1,3-butadiene has been suggested as the most likely product formed directly following C–S bond breaking, which is lately hydrogenated to form butene and butane. The reaction mechanism proposed by Schultz and Rahman [58] involves the perpendicular adsorption of thiophene molecule through the S atom on a S anion vacancy, followed by attack of the S–C bond by H from adjacent –OH groups, thus forming butadiene as primary product.

### 3.7.2. HDS of 4,6-DMDBT reaction

**3.7.2.1. Factors influencing the catalyst activity.** Alkyl-substituted DBTs are known to be more difficult to desulfurize than thiophene because of the steric hindrance of their alkyl groups hindering the S-atom interaction with the catalyst surface. Thus, our challenge in this work was to investigate if the catalyst modification with P could eliminate the planar configuration of alkyl-substituted DBT through the enhancement of hydrogenation, isomerization, dealkylation, and/or C–C bond scission reaction routes [45]. The effect of P incorporation on the Al-HMS substrate on the activity of the sulfided NiMo catalysts in the HDS of 4,6-DMDBT reaction was evaluated in a batch reactor at  $T=320^\circ\text{C}$  and  $P=5.5 \text{ MPa}$  of hydrogen pressure. A commercial NiMo/ $\gamma$ -Al<sub>2</sub>O<sub>3</sub> catalyst with a metal loading higher than that of the catalysts studied (16 vs. 12 wt.% Mo + Ni) was used as a reference.

**Fig. 11(a)** shows the specific reaction rates versus P-loading of the catalysts at a reaction time of 6 h. In good agreement with the HDS of thiophene results, it is noted that P-loading on the HMS substrate results in an increase of activity. The HDS activity of P-loaded sulfide catalysts follows a volcano-shaped curve, in line with the study of NiMoW/P/SBA-16 sulfide catalysts

[44]. The observed activity trend is: NiMo-1.0 > NiMo-1.5 > NiMo-0.5 > NiMo-0.0 > NiMo-2.0. Thus, the NiMo-1.0 catalyst turns out to be also the most active one, with an increment in activity of 72%. Compared with the commercial catalyst with higher metal loading, there are two catalysts (NiMo-1.0 and NiMo-1.5) showing higher activity than the reference one. Thus, the optimum performance is observed for the catalyst whose P-loading is close 1 wt.%, which is in good agreement with that reported for NiMo/P-MCM-41 catalysts [42]. As observed in the present work, the NiMo/P-MCM-41 sulfide catalysts demonstrated higher activity than the commercial NiMo/Al<sub>2</sub>O<sub>3</sub> catalyst when tested in HDS of 4,6-DMDBT in a batch reactor [42].

Besides, a linear dependence was observed between catalyst activity and the active phase dispersion derived from  $\text{H}_2$  chemisorption (Fig. 11(b)). Thus, the highest activity of the NiMo-1.0 catalyst appears to be related to the highest dispersion of the active phase among the catalysts studied and therefore to the formation of the smallest MoS<sub>2</sub> crystallites on the support surface (from HRTEM). Moreover, one might expect that the type of symmetry adopted by molybdenum and nickel ions in the Al-HMS-P(x) support surface might have some influence on the final catalytic response. In this sense, the oxide precursor of NiMo-1.0 sample showed the lowest amount of the Mo in tetrahedral coordination (from UV-vis). It is well known that tetrahedral molybdate (MoO<sub>4</sub>) species are more difficult to reduce and sulfide than a supported bulk MoO<sub>3</sub> acidic species. Additionally, a volcano-curve trend of the catalyst activity could also be explained considering a possible increase in the amount of nickel available to form the NiMoS active phase, as it was proposed by López Cordero et al. [52] for NiMo/P/Al<sub>2</sub>O<sub>3</sub> catalysts.

Finally, the detrimental effect of a large P-loading on the HDS activity of both NiMo-1.5 and NiMo-2.0 catalysts could be explained considering the sharp decrease in their specific area with respect to P-free sample (Table 2) and considering the large concentration of tetrahedral molybdenum species bound to the support surface (from DRS UV-vis). For those samples, the decrease of the active phase dispersion is consistent with a more difficult sulfidation of the support-linked tetrahedral Mo species (from TPS measurements, Fig. 5). This situation is similar to that observed by Anderson et al. [59] where the lower sulfidation degree has been achieved with Mo/USY sulfide catalyst containing a high concentration of tetrahedral molybdenum bound to the support. In addition, Herrera et al. [42] showed that an increase of P loading from 1.0 to 5.0 wt.% resulted in the formation of crystalline MoO<sub>3</sub> species, with subsequent formation of larger MoS<sub>2</sub> crystals during sulfidation of the NiMo/P-MCM-41 catalyst and a parallel activity drop in the 4,6-DMDBT HDS reaction.

**3.7.2.2. Factors influencing the selectivity.** Additional information on the P effect was obtained by analyzing selectivity data (calculated at the same 4,6-DMDBT conversion of ca. 30%) given in Table 5. For all the studied catalysts, including a commercial NiMo/Al<sub>2</sub>O<sub>3</sub> one, the products detected were dimethylbiphenyl (DMBP), methylcyclohexyltoluene (MCHT) and dimethylbicyclohexyl (DMBCH) being MCHT the main reaction product. Additionally, different isomers of the principal reaction products together with traces of the intermediate products such as tetrahydro- and hexahydro-dimethyldibenzothiophene (THD-MDBT and HHDMDBT, respectively) were detected. Based on the products detected, **Scheme 2** shows a simplified reaction mechanism of 4,6-DMDBT transformation over sulfided NiMo/Al-HMS-P catalysts. Under the reaction conditions employed, the HDS reaction of 4,6-DMDBT proceeds through two main reaction routes: direct desulfurization (DDS) leading to formation of 3,3'-DMBP and hydrogenation (HYD) reaction route producing tetrahydro- and hexahydro-DMDBT intermediates, and after S-elimination leading

**Table 5**

HDS of 4,6-DMDBT<sup>a</sup> specific rate, selectivity<sup>b</sup> and HYD/DDS selectivities ratio for NiMo-P(x) catalysts and NiMo/Al<sub>2</sub>O<sub>3</sub> reference catalyst.

Catalyst	Rate $\times 10^7$ [mol g <sup>-1</sup> cat. s <sup>-1</sup> ]	Selectivity (%) <sup>c</sup>			HYD/DDS <sup>c</sup>
		DMBP	DMDCHCH <sup>c</sup>	MCHT	
NiMo-0.0	4.0	29	5	66	2.44
NiMo-0.5	4.6	28	7	65	2.56
NiMo-1.0	6.9	21	14	65	3.70
NiMo-1.5	5.8	23	11	66	3.33
NiMo-2.0	3.8	37	4	59	1.69
NiMo/Al <sub>2</sub> O <sub>3</sub>	4.7	25	12	63	3.03

<sup>a</sup> The reaction conditions were:  $T=320^\circ\text{C}$ ;  $P=5.5$  MPa; 6 h of reaction time; a batch reactor.

<sup>b</sup> Achieved at 30% of DBT conversion: DMBP, dimethylbiphenyl; MCHT, methylcyclohexyltoluene; DMDCH, dimethyldicyclohexyl.

<sup>c</sup> DDS: direct desulfurization; HYD: hydrogenation pathway. The HYD/DDS selectivities ratio as calculated from selectivity of the products [(MCHT + DMDCH)/DMBP].

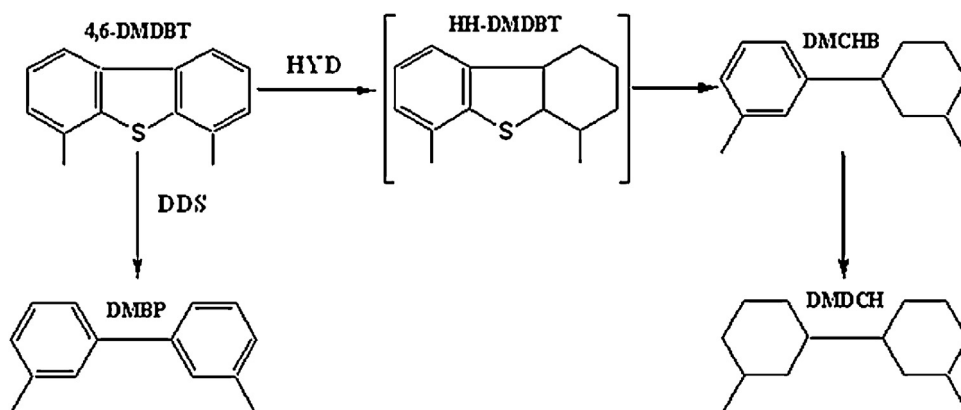
to the formation of MCHT and DMDCH. This is in good agreement with the CoMo/Ti-HMS-P(x) catalysts studied by us previously [45]. The isomerisation of 4,6-DMDBT also occurs but only small amounts of different isomers of the principal reaction products were detected for all the studied catalysts. Indeed, with the exception of NiMo-2.0, all the catalysts showed the same amount of Brønsted acid sites, as derived from FT-IR spectra of adsorbed pyridine (Table 4). Similarly to the NiMo-0.0 catalyst, the formation of different isomers in the main products was also observed over NiMo catalysts supported on Al-SBA-15 [33] and Al-SBA-16 sulfide catalysts [21].

It is generally accepted the hypothesis that  $\pi$ -adsorption favors hydrogenation reaction, whereas the sulfur adsorption is related to desulfurization reactions [60]. In general, it was found that the hidrodesulfurization via hydrogenation way over the catalyst was enhanced by the support modification with phosphorous, being in good agreement with the work of Herrera et al. [42]. Fig. 6 shows that (MCHT+DMDCH)/DMBP selectivity ratio (HYD/DDS ratio) increases with P loading up to 1.0 wt.%, which also presents better activity results, but then levels off. For all the studied catalysts, MCHT was the main reaction product (selectivity ca. 66%). Although the NiMo-2.0 catalyst shows the lowest selectivity toward this product (59%), at the same time, it can be noted that in all cases the HYD/DDS ratio was much higher than 1 (Table 5), indicating the predominance of the HYD reaction route over the HDS one. If the HYD/DDS ratios are plotted against the specific activity a linear increase is again observed (Fig. 11(a)), i.e., the most active catalyst presents better hydrogenating properties suggesting that the MoS<sub>2</sub> crystallites of this sample contain (a) the largest amount of promoted sites among the catalysts [61].

Interestingly, with the exception of NiMo-2.0 catalyst, there is a linear increase between 4,6-DMDBT transformation and HYD/DDS selectivity ratio (Fig. 12(a)) confirming that, for deep HDS catalysts,

the enhancement of their hydrogenation function is needed. For all the studied catalysts, the HYD/DDS selectivity ratio follows the trend: NiMo-1.0 > NiMo-1.5 > NiMo/Al<sub>2</sub>O<sub>3</sub> > NiMo-0.5 > NiMo-0.0 > NiMo-2.0 indicating that the two former catalysts show larger hydrogenation capability than the commercial one. The promotion of HYD route was explained in terms of the increase in catalyst acidity induced by H<sub>2</sub>S adsorption on the catalyst surface [62]. However, the reverse trend observed in this work between the HYD/DDS ratio and the catalyst acidity suggests a compromise between the enhancement of the catalyst HYD function and the decrease of the catalyst deactivation by decreasing the catalyst acidity. Indeed, the high acidity of NiMo-2.0 confirms the hypothesis that the introduction of high amounts of phosphate created medium strength acid sites, which in turn increases the total acidity of the support [37]. As a consequence, one might expect that coking could also increase.

The influence of the active phase dispersion on the specific reaction rate (expressed as activity per the catalyst surface area) is shown in Fig. 11(b). Thus, the decrease of the active phase dispersion may also explain the lowest HYD/DDS selectivity ratio of the NiMo-2.0 sample in the HDS of 4,6-DMDBT reaction (Fig. 12(b)). This is because the samples showing an inferior dispersion possess a lower amount of promoted active sites, which are widely accepted to decreases the formation of active sites for HYD reaction [61]. In this sense, phosphorous poisoning was explained by Bouwens et al. [63] in terms of the adsorption of phosphide (formed during the presulfiding treatment) on the anion vacancies. Although this explanation is also valid in this work, considering our previous HRTEM study on the NiMoW/SBA-16 sulfide catalysts with a high amount of P (2.0 wt.%) [44]. We strongly believe that the high presence of P<sub>2</sub>O<sub>5</sub> species on the support surface might force the formation of less active “onion-type” Mo(W)S<sub>2</sub> structures, which possess a low amount of rim/edge sites.



**Scheme 2.** Reaction scheme for the hydrodesulfurization of 4,6-DMDBT over sulfide NiMo/Al-HMS and NiMo/Al-HMS-P catalysts.

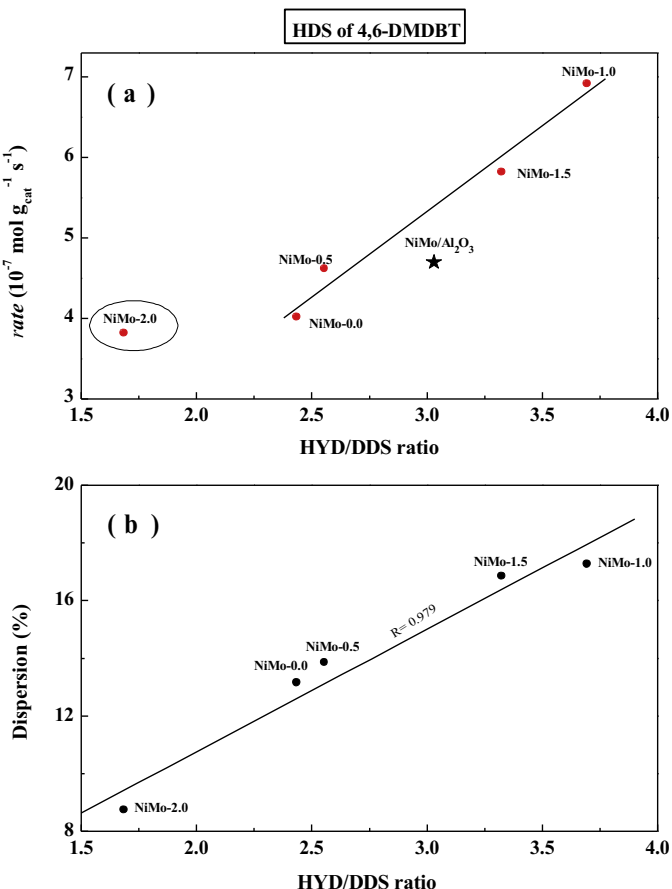


**Fig. 12.** HDS of 4,6-DMDBT DMBT ( $P=5.5$  MPa;  $T=320$  °C, reaction time of 6 h; a batch reactor) over NiMo/Al-HMS and NiMo/Al-HMS-P(x) sulfide catalysts. Catalytic activity against HYD/DDS selectivities ratio (a) and the influence of the active phase dispersion (from  $H_2$  chemisorption) on the HYD/DDS selectivities ratio (b).

#### 4. Conclusions

All catalysts showed changes in morphology and acidity induced by the presence of phosphate species on the support surface. The catalysts were tested in the HDS of thiophene and 4,6-DMDBT. The catalyst with nominal 1.0 wt.% P content exhibited the best performance in both HDS reactions. This was related to an increase in the active phase dispersion, as demonstrated by  $H_2$  chemisorption data, and to the enhancement amount of promoted sites in the active NiMoS phase. The HDS of 4,6-DMDBT reaction over all catalysts proceeds toward direct desulfurization, hydrogenation and isomerization reaction routes being inhibited dealkylation and/or C–C bond scission reaction routes. Concerning the HDS of thiophene, the increase of the catalyst acidity led to the formation of butadiene and a diminished hydrogenation of olefins (formation of butane) while no olefin chain-branched occurred.

#### Acknowledgments

The authors are grateful to Eric Flores, Eloisa Aparicio, David Dominguez, Jose Antonio Díaz, Francisco Ruiz and Israel Gradilla for their technical assistances and CONACYT projects 152012, 155388 and 117373 for the financial supports.

#### References

- [1] U.S. Environmental Protection Agency, (<http://www.epa.gov/otaq/gasoline.htm>), (<http://www.epa.gov/otaq/diesel.htm>).
- [2] EU Regulations, (<http://www.dieselnet.com/standards/eu/fuel.php>).
- [3] J.D.K. Bishop, C.J. Axon, M. Tran, D. Bonilla, D. Banister, M.D. McCulloch, *Fuel* 99 (2012) 88–105.
- [4] H. Topsøe, B.S. Clausen, F.E. Massoth, J.R. Anderson, M. Boudart (Eds.), *Hydrotreating Catalysts*, Springer Verlag, Berlin Heidelberg, 1996, pp. 1–269.
- [5] M. Grings, B.C. Gates, *Ind. Eng. Chem. Res.* 30 (1991) 2021–2058.
- [6] D. Laurenti, B. Phung-Ngoc, C. Roukoss, E. Devers, K. Marchand, L. Massin, L. Lemaitre, C. Legens, A.A. Quoineaud, M. Vrinat, *J. Catal.* 297 (2013) 165–175.
- [7] S.Y. Yu, W. Li, E. Iglesia, *J. Catal.* 187 (1999) 257–261.
- [8] B. Pawelec, R. Mariscal, R.M. Navarro, J.M. Campos-Martin, J.L.G. Fierro, *Appl. Catal., A: Gen.* 262 (2004) 155–166.
- [9] R. Zhao, C. Yin, H. Zhao, C. Liu, *Fuel Process. Technol.* 81 (2003) 201–209.
- [10] C. Sepulveda, V. Bellière, D. Laurenti, N. Escalona, R. García, C. Geantet, M. Vrinat, *Appl. Catal., A: Gen.* 393 (2011) 288–293.
- [11] D. Trong On, D. Desplantier-Giscard, C. Danumah, S. Kaliaguine, *Appl. Catal., A: Gen.* 253 (2003) 545–602.
- [12] A. Taguchi, F. Schüth, *Microporous Mesoporous Mater.* 77 (2005) 1–45.
- [13] S. Kawi, S.C. Shen, P.L. Chew, *J. Mater. Chem.* 12 (2002) 1582–1586.
- [14] A. Tuel, *Microporous Mesoporous Mater.* 27 (1999) 151–169.
- [15] T.A. Zepeda, B. Pawelec, J.L.F. Fierro, A. Olivas, S. Fuentes, T. Halachev, *Microporous Mesoporous Mater.* 111 (2008) 157–170.
- [16] T. Chiranjeevi, P. Kumar, M.S. Rana, S.K. Maity, G. Murali Dhar, T.S.R. Prasada Rao, *Microporous Mesoporous Mater.* 44–45 (2001) 547–556.
- [17] T. Chiranjeevi, P. Kumar, M.S. Rana, G. Murali Dhar, T.S.R. Prasada Rao, *J. Mol. Catal. A: Chem.* 181 (2002) 109–117.
- [18] M. Alibouri, S.M. Ghoreishi, H.R. Aghabozorg, *Ind. Eng. Chem. Res.* 48 (2009) 4283–4292.
- [19] M. Alibouri, S.M. Ghoreishi, H.R. Aghabozorg, *J. Supercrit. Fluids* 49 (2009) 239–248.
- [20] R. Huirache-Acuña, B. Pawelec, C.V. Loricera, E.M. Rivera-Muñoz, R. Nava, B. Torres, J.L.G. Fierro, *Appl. Catal., B: Environ.* 125 (2012) 473–485.
- [21] T. Klimova, L. Lizama, J.C. Amezua, P. Roquero, E. Terrés, J. Navarrete, J.M. Domínguez, *Catal. Today* 98 (2004) 141–150.
- [22] M.V. Landau, L. Vrádman, M. Herskowitz, Y. Koltypin, A. Gedanken, *J. Catal.* 201 (2001) 22–36.
- [23] K.C. Park, D.J. Yim, S.K. Ihm, *Catal. Today* 74 (2002) 281–290.
- [24] T. Klimova, M. Calderón, J. Ramírez, *Appl. Catal., A: Gen.* 240 (2003) 29–40.
- [25] M.J.B. Souza, B.A. Marinkovic, P.M. Jardim, A.S. Araujo, A.M.G. Pedrosa, R.R. Souza, *Appl. Catal., A: Gen.* 316 (2007) 212–218.
- [26] Y. Wang, S.K. Ihm, G. Lu, *Catal. Lett.* 92 (2007) 165–173.
- [27] A.M. Venezia, R. Murania, V. La Parola, B. Pawelec, J.L.G. Fierro, *Appl. Catal., A: Gen.* 383 (2010) 211–216.
- [28] K. Segawa, K. Takahashi, S. Satoh, *Catal. Today* 63 (2000) 123–132.
- [29] S. Zeng, J. Blanchard, M. Breysse, Y. Shi, X. Su, H. Nie, D. Li, *Appl. Catal., A: Gen.* 294 (2005) 59–67.
- [30] G. Muthu Kumaran, S. Garg, K. Soni, M. Kumar, L.D. Sharma, G. Murali Dhar, K.S. Rama Rao, *Appl. Catal., A: Gen.* 305 (2006) 123–129.
- [31] G. Muthu Kumaran, S. Garg, K. Soni, M. Kumar, L.D. Sharma, K.S. Rama Rao, G. Murali Dhar, *Ind. Eng. Chem. Res.* 46 (2007) 4747–4754.
- [32] G. Macías Esquivel, J. Ramírez, A. Gutiérrez-Alejandre, *Catal. Today* 148 (2009) 36–41.
- [33] T. Klimova, J. Reyes, O. Gutiérrez, L. Lizama, *Appl. Catal., A: Gen.* 335 (2008) 159–171.
- [34] M. Gómez-Cazalilla, A. Infantes-Molina, R. Moreno-Tost, P.J. Maireles-Torres, J. Mérida-Robles, E. Rodríguez-Castellón, A. Jiménez-López, *Catal. Today* 143 (2009) 137–144.
- [35] R. Huirache-Acuña, B. Pawelec, E. Rivera-Muñoz, R. Nava, J. Espino, J.L.G. Fierro, *Appl. Catal., B: Environ.* 92 (2009) 168–184.
- [36] R. Iwamoto, J. Grimblot, *Adv. Catal.* 44 (2000) 417–503.
- [37] A. Stanislaus, M. Absi-Halabi, A. Al-Doloma, *Appl. Catal.* 39 (1988) 239–253.
- [38] C.W. Fitz, H.F. Rase, *Ind. Eng. Chem. Prod. Dev.* 22 (1983) 40–44.
- [39] S. Eijlsbouts, J.N.M. van Gestel, J.A.R. van Veen, V.H.J. de Beer, R. Prins, *J. Catal.* 131 (1991) 412–432.
- [40] J.M. Lewis, R.A. Kydd, P.M. Boorman, P.H. Van Rhyn, *Appl. Catal., A: Gen.* 84 (1992) 103–121.
- [41] J.M. Lewis, R.A. Kydd, *J. Catal.* 136 (1992) 478–486.
- [42] J.M. Herrera, J. Reyes, P. Roquero, T. Klimova, *Microporous Mesoporous Mater.* 83 (2005) 283–291.
- [43] R. Nava, B. Pawelec, J. Morales, R.A. Ortega, J.L.G. Fierro, *Microporous Mesoporous Mater.* 118 (2009) 189–201.
- [44] M.A. Guzmán, R. Huirache-Acuña, C.V. Loricera, J.R. Hernández, N. Díaz de León, J.A. de los Reyes, B. Pawelec, *Fuel* 103 (2013) 321–333.
- [45] B. Pawelec, J.L.G. Fierro, A. Montesinos, T.A. Zepeda, *Appl. Catal., B: Environ.* 80 (2008) 1–14.
- [46] T. Halachev, J.A. de los Reyes, C. Araujo, L. Dimitrov, G. Cordoba, in: B. Delmon, G.F. Froment, P. Grange (Eds.), *Hydrotreatment and Hydrocracking of Oil Fractions, Studies in Surface Science and Catalysis*, Elsevier, 1999, p. 401.
- [47] R. Nava, A. Infantes-Molina, P. Castaño, R. Gui-López, B. Pawelec, *Fuel* 90 (2011) 2726–2737.
- [48] R. Nava, J. Morales, G. Alonso, C. Ornelas, B. Pawelec, J.L.G. Fierro, *Appl. Catal., A: Gen.* 321 (2007) 58–70.
- [49] B. Pawelec, S. Damyanova, R. Mariscal, J.L.G. Fierro, I. Sobrados, J. Sanz, L. Petrov, *J. Catal.* 223 (2004) 86–97.
- [50] S. Gontier, A. Tuel, *Zeolites* 15 (1995) 601–610.
- [51] O.Y. Gutiérrez, T. Klimova, *J. Catal.* 281 (2011) 50–62.
- [52] R. López Cordero, A. López Agudo, *Appl. Catal., A: Gen.* 202 (2000) 23–35.

- [53] R. López Cordero, F.J. Gil Llambias, A. López Agudo, *Appl. Catal.* 74 (1991) 125–136.
- [54] J.W. Niemantsverdriet, *Spectroscopy in Catalysis. An Introduction*, third ed., Wiley-VCH, 2007, pp. 217–249 (Chapter 8).
- [55] B. Chakraborty, B. Viswanathan, *Catal. Today* 49 (1999) 253–260.
- [56] G. Busca, *Catal. Today* 41 (1–3) (1998) 191–206.
- [57] C.A. Emeis, *J. Catal.* 141 (1993) 347–354.
- [58] H. Schultz, N.M. Rahman, *Stud. Surf. Sci. Catal.* 75 (1993) 585–595.
- [59] J.A. Anderson, B. Pawelec, J.L.G. Fierro, *Appl. Catal., A: Gen.* 99 (1993) 55–70.
- [60] V. Meille, E. Schultz, M. Lemaire, M. Vrinat, *J. Catal.* 170 (1997) 29–36.
- [61] M. Daage, R.R. Chianelli, *J. Catal.* 149 (1994) 414–427.
- [62] E. Lecrenay, K. Sakanishi, I. Mochida, *Catal. Today* 39 (1997) 13–20.
- [63] S.M.A.M. Bouwens, J.P.R. Vissers, V.H.J. de Beer, R. Prins, *J. Catal.* 112 (1988) 401–410.